

High spin temperatures at large impact parameters: Ionisation in the outskirts of galaxies

S. J. Curran

School of Chemical and Physical Sciences, Victoria University of Wellington, PO Box 600, Wellington 6140, New Zealand
e-mail: Stephen.Curran@vuw.ac.nz

January 22, 2020

ABSTRACT

By including the most recent observations of H I 21-cm absorption through nearby galactic discs, we confirm our previous assertion that there is an anti-correlation between the abundance of cool neutral atomic gas and impact parameter. Comparing the measured neutral hydrogen column densities of the sample with the absorption strength, we find a peak in the mean spin temperature of $\langle T_{\text{spin}}/f \rangle \approx 2310$ K at an impact parameter of $\rho \approx 14$ kpc, with $\langle T_{\text{spin}}/f \rangle \gg 1000$ K in the remainder of the disc. This is significantly different to the spin temperature distribution in the Milky Way, which exhibits a constant $\approx 250 - 400$ K over $\rho = 8 - 25$ kpc. The measured column densities may, however, suffer from beam dilution, which we show appears to be the case for the observations of H I 21-cm emission in which the beam subtends radii of ≥ 10 kpc. We therefore applied the column density profile of the Milky Way, in addition to the mean of the sample, observed at sufficiently high resolution, and the mean profile for the nearby $\sim 10^{12} M_{\odot}$ galaxies in the IllustrisTNG simulations. All of the models yield a peak in the mean spin temperature at similar impact parameters ($r \approx 10 - 15$ kpc) as the measured column densities. These radii are similar to those of the spiral arms where H II regions are often concentrated. We therefore suggest that the elevated spin temperatures trace the H II regions observed in the outer disc of many spiral galaxies.

Key words. galaxies: structure – galaxies: ISM – ISM: H II regions – galaxies: spiral – radio lines: galaxies

1. Introduction

Absorption of the 21-cm flux from distant radio sources through the discs of nearby galaxies provides information on the neutral hydrogen (H I) gas. In particular, a comparison of the absorption strength to the total H I column density yields the spin temperature of the gas, which is a measure of the population of the upper hyperfine level relative to the lower level. This can be increased via excitation by 21-cm absorption (Purcell & Field 1956), excitation above the ground state by Lyman- α absorption (Field 1959) and collisional excitation (Bahcall & Ekers 1969). The spin temperature gives the fraction of the cold neutral medium (CNM, where $T \sim 100$ K and $n \sim 10 \text{ cm}^{-3}$) to the warm neutral medium (WNM, where $T \sim 2000$ K and $n \sim 0.4 \text{ cm}^{-3}$, Sofue 2018). Both the total gas density (e.g. Toomre 1963) and fraction of cool neutral gas (Curran et al. 2016) exhibit a decrease in abundance with the galactocentric radius. The latter, based on the then 90 sight-lines searched for H I 21-cm absorption, has, however, since been refuted by subsequent studies (Borthakur 2016; Dutta et al. 2017). A flat 21-cm absorption strength in conjunction with a decreasing column density would result in temperature climb outwards across the disc. This runs contrary to what is seen in the Milky Way, where the mean spin temperature maintains $\langle T_{\text{spin}} \rangle = 250 - 400$ K over radii of $8 - 25$ kpc (Dickey et al. 2009).

From the decrease in 21-cm absorption strength with the impact parameter, Curran et al. (2016) find the mean spin temperature to peak, with $\langle T_{\text{spin}} \rangle \approx 2900$ K, at $\rho \approx 10$ kpc. This, however, was based on a sample of just 27 sight-lines with measured column densities. Additionally, given that spin temperatures of ≈ 500 K and ≈ 200 K were found for the inner and outer disc,

respectively, this was deemed to be consistent with the Galactic values. With these new data, the number of sight-lines is now 143, for which 39 have column density measurements. Here we add the new data to the previous, confirming that the 21-cm absorption strength is anti-correlated with impact parameter, in addition to using the column densities to determine the mean spin temperature of the gas across the disc.

2. Analysis

2.1. Absorption strength versus impact parameter

The addition of subsequent data (Borthakur 2016; Dutta et al. 2017; Allison 2020) to that used in Curran et al. (2016)¹, brings the number of sight-lines from 90 to 143. This comprises 22 detections of 21-cm absorption and 121 upper limits. In order to include these, we re-sample the limits to a common spectral resolution/profile width of 10 km s^{-1} (see Curran 2012) and then flag these as censored data points using the *Astronomy SURVival Analysis* (ASURV) package (Isobe et al. 1986).

Plotting the integrated optical depth versus the impact parameter (Fig. 1), a generalised non-parametric Kendall-tau test gives a probability of $P(\tau) = 2.87 \times 10^{-4}$ of the observed $\int \tau dv$ - ρ anti-correlation arising by chance. Assuming Gaussian statistics, this is significant at $S(\tau) = 3.63\sigma$, cf. 3.31σ previously (Curran et al. 2016). Neither Borthakur (2016) nor Dutta et al.

¹ Compiled from Haschick & Burke (1975); Boisse et al. (1988); Corbelli & Schneider (1990); Carilli & van Gorkom (1992); Kanekar et al. (2002); Hwang & Chiou (2004); Borthakur et al. (2010, 2011, 2014); Gupta et al. (2010, 2013); Srianand et al. (2013); Reeves et al. (2015, 2016); Zwaan et al. (2015); Dutta et al. (2016).

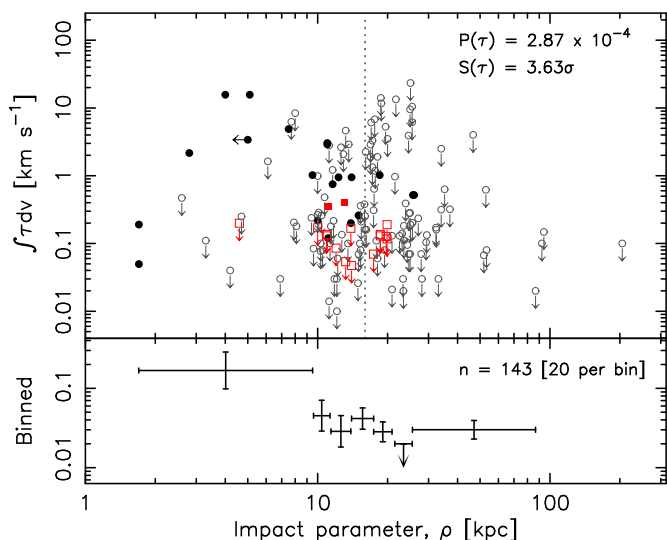


Fig. 1. Velocity integrated optical depth versus the impact parameter for all of the published searches. The circles represent the previous data (Curran et al. 2016 and references therein) and the squares the data since (Borthakur 2016; Dutta et al. 2017; Allison 2020). The downward arrows signify the 3σ upper limits and the dotted vertical line shows the median impact parameter. The bottom panel shows the binned values, including the limits via the Kaplan–Meier estimator, in equally sized bins. The horizontal error bars show the range of points in the bin and the vertical error bars the 1σ uncertainty in the mean value.

(2017) find a strong correlation, although the former only test their sample of one 21-cm absorption detection and 15 non-detections (all at $\rho < 20$ kpc) and the latter limit their impact parameters to $\rho < 30$ kpc, resulting in $S(\tau) = 2.42\sigma$.

The $\int \tau dv - \rho$ dependence is confirmed via the detection rates above and below the median impact parameter of $\rho = 16$ kpc. At $\rho \leq 16$ kpc there are 19 detections and 53 non-detections, giving 26.4 per-cent detection rate. At $\rho > 16$ kpc there are three detections and 68 non-detections. Based on a likelihood of $p = 0.264$, the binomial probability of obtaining three detections or fewer out of 71 sight-lines is 6.16×10^{-6} , which is significant at 4.50σ .

2.2. Spin temperature versus impact parameter

Several of the sight-lines have been detected in 21-cm emission from which the column density can be obtained from the brightness temperature of the line emission, T_b [K]. In the optically thin regime ($\tau \lesssim 0.3$) the column density, N_{HI} [cm^{-2}] is given by

$$N_{\text{HI}} = 1.823 \times 10^{18} \int T_b dv, \quad (1)$$

and in absorption the column density is related to the spin temperature, T_{spin} [K], via

$$N_{\text{HI}} = 1.823 \times 10^{18} \frac{T_{\text{spin}}}{f} \int \tau dv, \quad (2)$$

where f is the covering factor; the fraction of the background flux intercepted by the absorbing gas. Thus, the comparison of the velocity integrated optical depth with the column density yields the spin temperature degenerate with the covering factor, T_{spin}/f . For unresolved galaxies detected in 21-cm absorption at non-zero redshifts, the covering factor is dependent upon the relative absorber and emitter cross-sections as well as the redshift

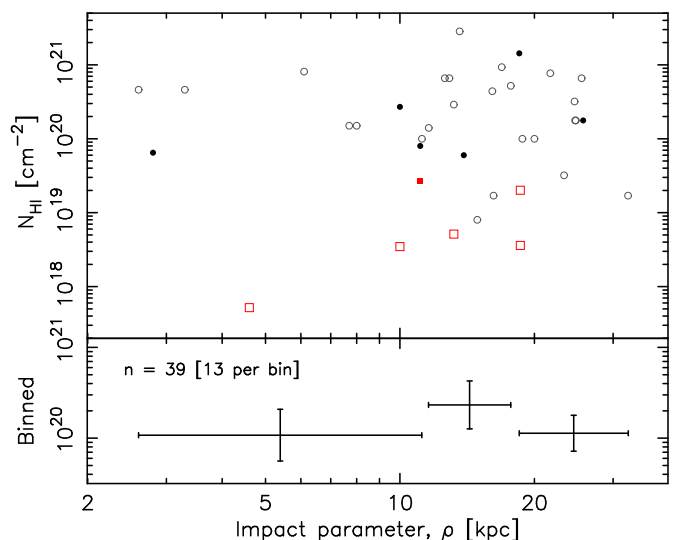


Fig. 2. Column density versus the impact parameter for the sight-lines detected in 21-cm emission.

of the background source (Curran 2012). Given, that here the absorption is occurring through a nearby resolved disc, it is fair to assume that all of the background flux is intercepted, giving $f \approx 1$.

2.2.1. Measured column densities

For 39 of the sight-lines 21-cm emission has been detected, giving the H I column density. Where this is not given (e.g. Borthakur 2016), we obtain the brightness temperature from the H I mass, M_{HI} , via the integrated flux density of the emission (e.g. Rohlfs & Wilson 2000)

$$M_{\text{HI}} = 236 D_L^2 S_{\text{int}}, \quad \text{where } S_{\text{int}} = \frac{2k\Omega_b}{\lambda^2} \int T_b dv, \quad (3)$$

D_L is the luminosity distance [Mpc], S_{int} the integrated flux of the line [mJy km s^{-1}], k the Boltzmann constant, Ω_b the beam solid angle of the telescope at the wavelength λ [m] and $\int T_b dv$ the velocity integrated brightness temperature [K km s^{-1}].

In Fig. 2 we show the distribution of column density with impact parameter for the sight-lines with detected 21-cm emission. From this, we see that the column density is fairly consistent out to $\rho \approx 25$ kpc, with a possible elevation at ≈ 15 kpc. In Fig. 3, we show the resulting spin temperatures, which exhibits a similar T_{spin}/f bump as previously (Curran et al. 2016), the binning of the data giving $\langle T_{\text{spin}}/f \rangle = 1370_{-700}^{+1440}$ K at $\rho \approx 5$ kpc, $\langle T_{\text{spin}}/f \rangle = 2310_{-670}^{+940}$ K at $\rho \approx 14$ kpc and $\langle T_{\text{spin}}/f \rangle = 1100_{-220}^{+470}$ K at $\rho \approx 25$ kpc. These temperatures are considerably higher than in the Milky Way (Sect. 1).

Determining the spin temperature through the comparison of Eqs. 1 and 2 relies upon the same sight-line being probed, which may not be the case here: In absorption we observe a ‘pencil-beam’ through the gas, whereas for emission we observe over the whole telescope beam, which results in dilution if the beam size exceeds that of the emitting gas ($r_{\text{beam}} > r_{\text{gas}}$). The linear extent of the beam is given by $r_{\text{beam}} = \theta_{\text{beam}} D_A$, where θ_{beam} is the angular beam size [radians] and D_A the angular diameter distance (e.g. Peacock 1999) to the galaxy [kpc], obtained from the redshift (Fig. 4). Showing N_{HI} versus r_{beam} in Fig. 5, we see a clear dependence between the measured column density and the beam width.

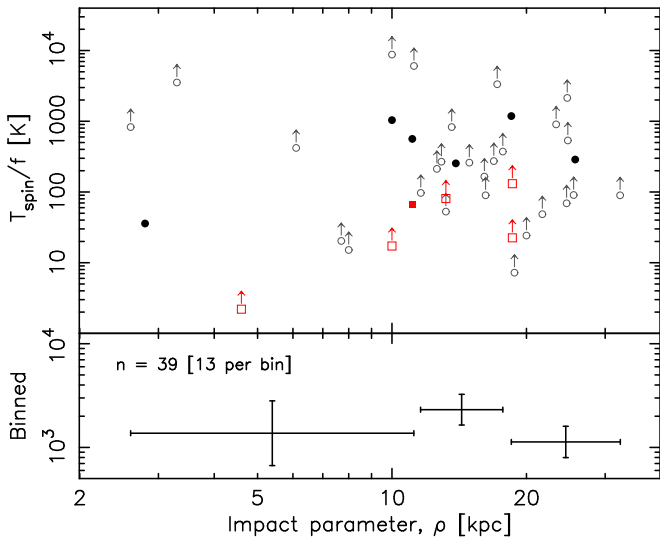


Fig. 3. Spin temperature/covering factor obtained from the column density (Fig. 2), versus the impact parameter. The upward arrows signify lower limits.

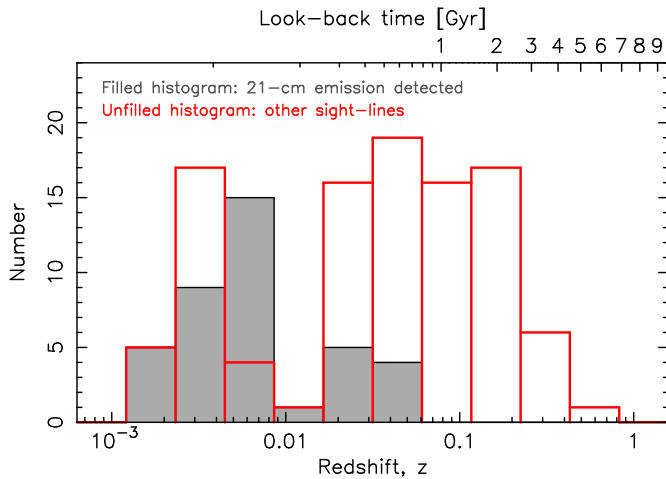


Fig. 4. Redshift distribution of the target galaxies. The galaxies span the redshift range $0 \leq z \leq 0.4367$, with 21-cm emission being detected to $z = 0.0462$ (filled histogram).

2.2.2. Galactic column density

In order to bypass the effect of beam dilution on the column density, we can apply well constrained profiles in similar galaxies to our sample. One option is to use the Milky Way, where the total (north and south, Kalberla & Dedes 2008) disc distribution is shown in Fig. 6. We overlay the mean integrated optical depths of the 21-cm absorption for a constant spin temperature of $T_{\text{spin}}/f \approx 4000$ K, which traces the column density out to $r \approx 20$ kpc, beyond which the spin temperature decreases due to the edge of the stellar disc being reached. These spin temperatures are much higher than observed in the Milky Way (Dickey et al. 2009) and, unlike the Galactic values, appear to be further elevated at $r \approx 10$ kpc.

Using both the exponential fit (for $12.5 \leq r \leq 35$ kpc, Kalberla & Kerp 2009) and the log-polynomial fit (for $r \leq 40$ kpc), which provides a better trace of the inner disc, we show the spin temperature profile in Fig. 7. Where the radii overlap, these give similar results and, again, a peak in the spin temperature of $T_{\text{spin}}/f \approx 15000$ K at $r \approx 10 - 15$ kpc, with the inner and

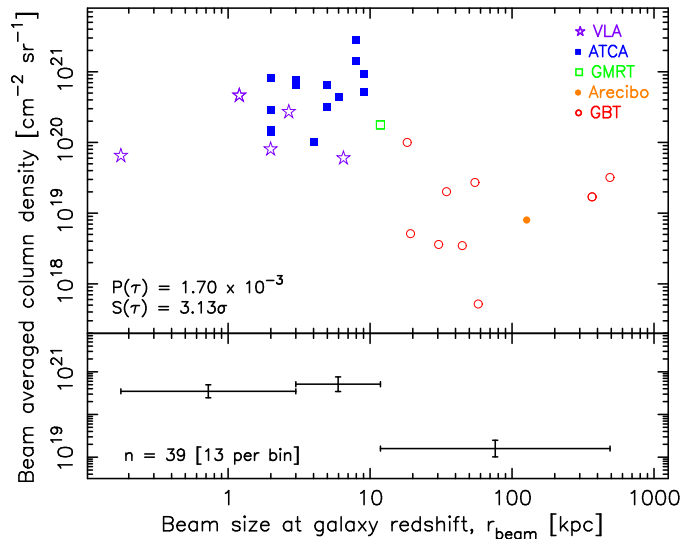


Fig. 5. Column density measured across the telescope beam versus the linear extent of the beam for the sight-lines detected in 21-cm emission. The telescopes used are the Very Large Array (VLA, Carilli & van Gorkom 1992; Borthakur et al. 2011, 2014), the Australia Telescope Compact Array (ATCA, Reeves et al. 2015, 2016), the Giant Metre-Wave Radio Telescope (GMRT, Dutta et al. 2016), the Arecibo telescope (Corbelli & Schneider 1990) and the Green Bank Telescope (GBT, Haschick & Burke 1975; Borthakur et al. 2011; Borthakur 2016).

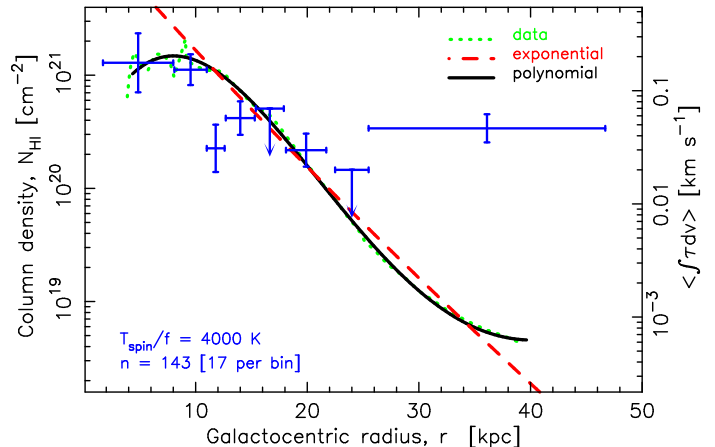


Fig. 6. Radial column density distribution of the Milky Way (total disc, Kalberla & Dedes 2008) overlain with the exponential fit to the $r \geq 12.5$ kpc data (Kalberla & Kerp 2009) and a log-polynomial to all of the data. The error bars show the column density of the 21-cm absorption for $T_{\text{spin}}/f = 4000$ K (right axis).

outer stellar disc having temperatures $T_{\text{spin}}/f \approx 3000 - 5000$ K (see Table 1).

Dispensing with the assumed column density profile, we can compare the mean 21-cm absorption strengths (Fig. 1) directly with those of the Milky Way. Dickey et al. (2009) give these in terms of $\int \tau_{\text{d}}/L$, where the path length $L = N_{\text{H}1}/n_{\text{H}1}$ and $n_{\text{H}1}$ is the volume density of the gas. From the column density (Fig. 6) and mid-plane volume density profiles (Kalberla & Dedes 2008) of the Milky Way, we obtain the path length distribution shown in Fig. 8, which exhibits the flaring of the scale-height of the H I disc (Kalberla et al. 2007). Showing the resulting integrated optical depths in Fig. 9, we see that the mean sample strengths are significantly weaker than the Galactic values, especially in the inner disc. For a given column density profile this will result

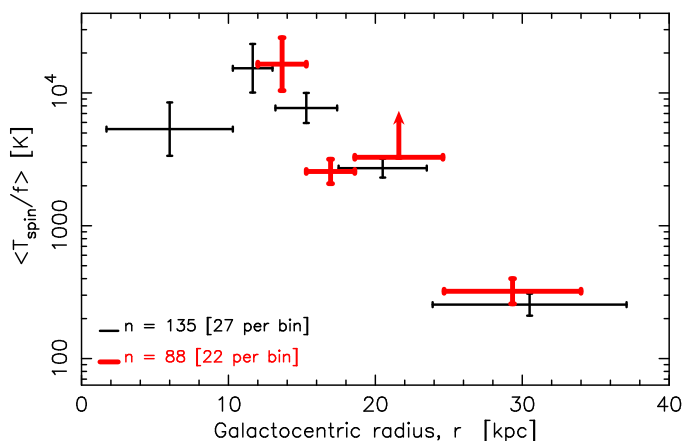


Fig. 7. Spin temperature/covering factor values obtained from the polynomial (thin bars) and exponential (thick bars) fits to the Galactic column density distribution (Fig. 6).

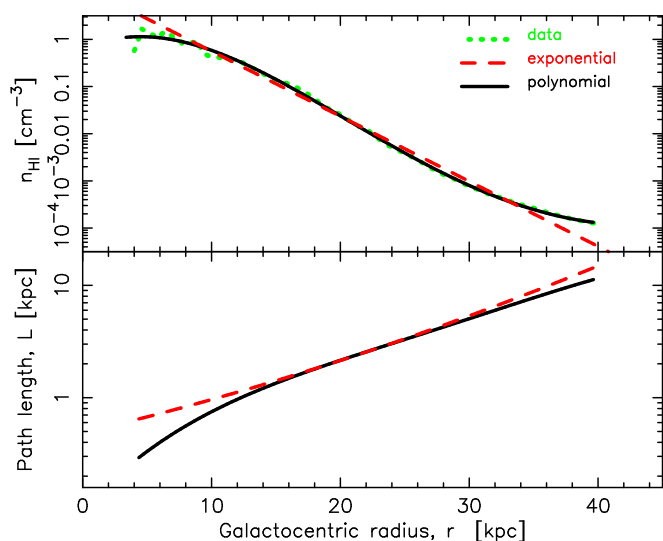


Fig. 8. Top: Volume density profile of the Milky Way (total disc, Kalberla & Dedes 2008), overlain with the exponential and a log-polynomial fit. Bottom: The resulting path length profile.

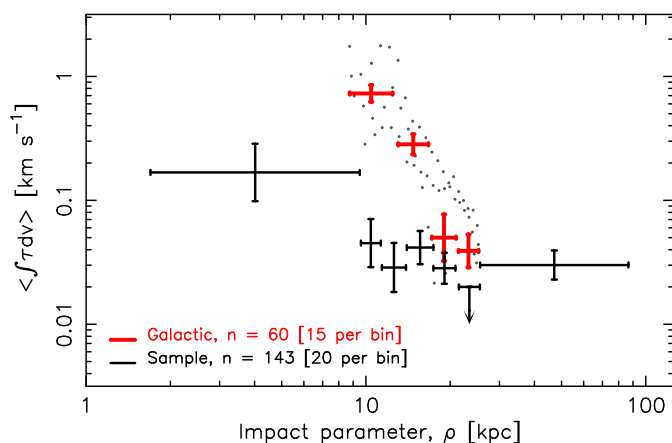


Fig. 9. Binned mean velocity integrated optical depth of the sample (thin bars) in comparison to the Milky Way: The data from each of the Canadian Galactic Plane Survey (CGPS, Taylor et al. 2003), the Southern Galactic Plane Survey (SGPS, McClure-Griffiths et al. 2005) and the VLA Galactic Plane Survey (VGPS, Stil et al. 2006) are shown as points, with the thick bars showing the binned values.

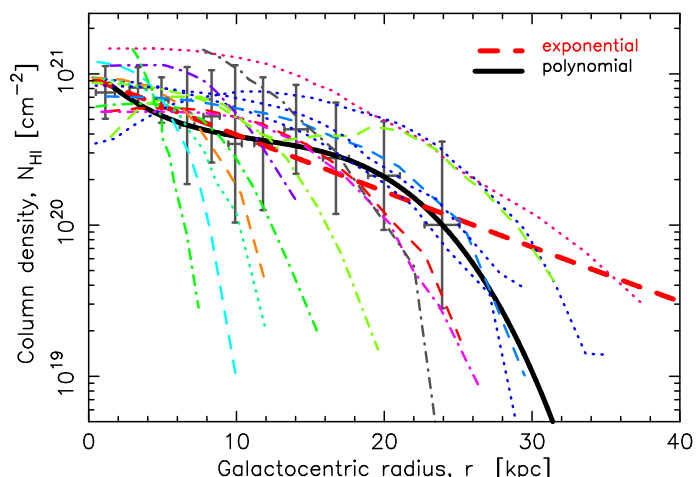


Fig. 10. H I column density profiles from the high resolution observations of Reeves et al. (2015, 2016). The error bars show the mean values and the $\pm 1\sigma$ uncertainties. The thick unbroken curve shows the $(1/\sigma)$ weighted log-polynomial fit and the broken line the weighted exponential fit to the mean values.

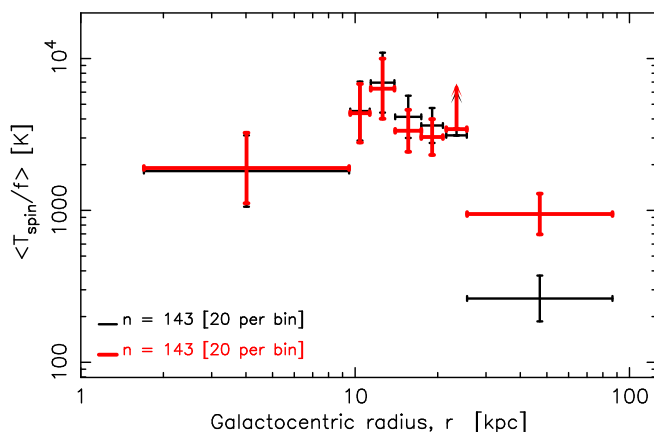


Fig. 11. As per Fig. 7 but for the mean sample column density distribution (Fig. 10).

in higher spin temperatures for the sample, thus indicating that a very different profile is required to yield temperatures similar to that in the Milky Way.

2.2.3. Mean sample column density

Another option for the column density profile is to use those of the sample itself, which we show in Fig. 10, where available.² The profiles are very diverse and so we model the column density distribution via a weighted log-polynomial and a weighted exponential fit to the mean values. These show reasonable agreement out to $r \approx 20$ kpc, beyond which the polynomial appears to provide the best mean trace. In Fig. 11, we show the spin temperature profile generated by both fits. Again, these are higher than in the Milky Way, but lower than that obtained using the Galactic column density distribution. There is, however, a similar peak in the spin temperature, $T_{\text{spin}}/f = 7000^{+4000}_{-2500}$ K at $r \approx 12$ kpc, with $T_{\text{spin}}/f \approx 2000 - 3000$ K in the remainder of the stellar disc.

We acknowledge that this is based upon the mean column density distribution, where the individual cases differ drastically. Ideally, we would determine the spin temperature from the 21-

² From high resolution observations with the ATCA (Reeves et al. 2015, 2016).

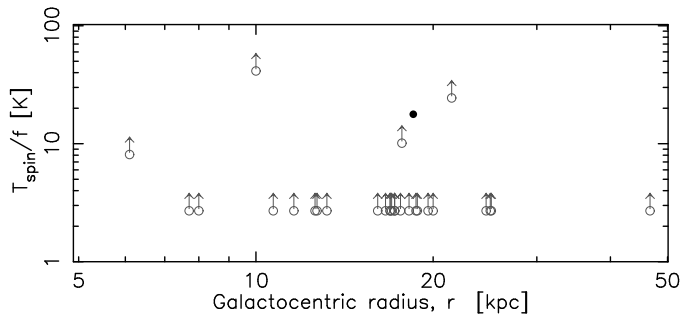


Fig. 12. Spin temperature/covering factor values at various impact parameters for the 21-cm observations and column density profiles of Reeves et al. (2015, 2016). The symbols are per Fig. 3, where the limits with $T_{\text{spin}}/f < T_{\text{CMB}}$ have been capped at $T_{\text{spin}}/f \geq 2.7$ K.

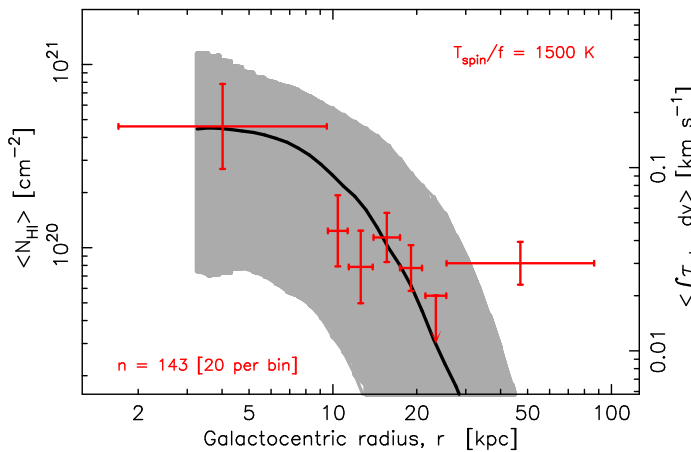


Fig. 13. Mean H I column density from an ensemble of $z = 0$ galaxies from the TNG (left axis), with the integrated column density of the 21-cm absorption overlain (for $T_{\text{spin}}/f = 1500$ K, right axis). The shaded region shows the 16th and 84th percentiles (1σ) of the population variation in the TNG.

cm absorption strength scaled by the relevant column density for each individual sight-line. Doing this for the high resolution observations (Fig. 12), we see, however, that due, partly at least, to the high impact parameters probed, this yields almost exclusive limits, most of which are relatively weak. Thus, we have little choice but to use the averaged 21-cm absorption strengths (Fig. 1), normalised by a mean column density distribution in order to yield a (mean) spin temperature profile.

2.2.4. Simulated column density

Both the column density profiles of the Milky Way and the mean sample yield spin temperatures much higher than Galactic values. This could be due to the relatively high column densities, with $N_{\text{H I}} \sim 10^{21} \text{ cm}^{-2}$ at $r \approx 0$ in both cases. Lower column densities can be obtained from the mean profile generated by the IllustrisTNG simulations for the 567 $z = 0$ galaxies with $\log_{10} M = 11.8 - 11.9 M_{\odot}$ (Nelson et al. 2019, Fig. 13). Comparing the 21-cm absorption strength with the column density distribution, we find, as for the Galactic distribution (Fig. 6), that the profile is well fit for a constant T_{spin}/f , besides from a peak at $r \approx 12$ kpc and a drop in spin temperature beyond the stellar disc. However, the spin temperature required is much lower than the $T_{\text{spin}}/f \approx 4000$ K from the Galactic $N_{\text{H I}}$ distribution, with the profile (Fig. 14) giving $T_{\text{spin}}/f \approx 1200 - 1500$ K

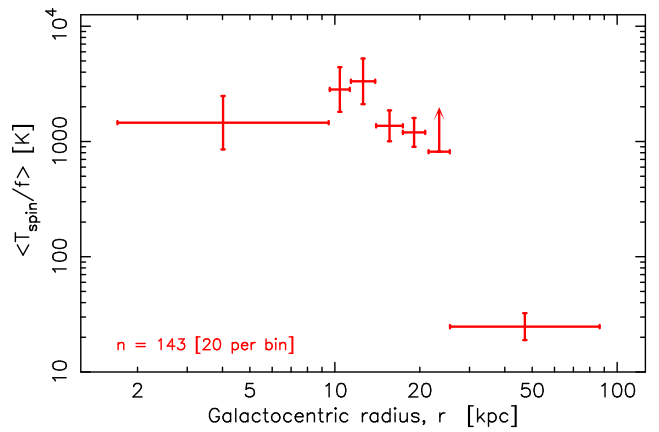


Fig. 14. Spin temperature/covering factor values obtained from the mean TNG column density profile (Fig. 13).

in the stellar disc, with the $r \approx 12$ kpc peak persisting (with $T_{\text{spin}}/f = 3300_{-1200}^{+1900}$ K, Fig. 14).

3. Discussion

All of the above models (summarised in Table 1) lead to significantly higher spin temperatures than in the Milky Way, with each exhibiting a peak at $r \approx 12$ kpc. Beyond this, the decrease in spin temperature is most likely due to the H I disc extending beyond the stellar disc (e.g. Curran et al. 2008; Walter et al. 2008). However, temperatures similar to that within the inner Milky Way are not reached until $r \approx 30$ kpc. The high T_{spin}/f values could be accounted for by covering factors $f \sim 0.1$, although we expect $f \sim 1$ for the absorption of unresolved quasar emission through a resolved disc.

Regarding the peak, in spiral galaxies, including the Milky Way (Lockman 1976), the ionised gas (H II) regions are concentrated in the spiral arms, at radii of up to $r \approx 15$ kpc (e.g. Hodge 1969; Hodge & Kennicutt 1983; James et al. 2009), believed to be caused by OB stars (Morgan et al. 1953).³ The ionising ($\lambda \leq 912 \text{ \AA}$) photon rate from each star is given by $Q_{\star} \equiv \int_{\nu_0}^{\infty} (L_{\nu}/h\nu) d\nu$, where $\nu_0 = 3.29 \times 10^{15} \text{ Hz}$, L_{ν} is the specific luminosity at frequency ν and h the Planck constant. For a radiative recombination rate coefficient of α_{B} and proton and electron volume densities n_{p} and n_{e} , respectively, the equilibrium between the photo-ionisation and recombination of protons and electrons is (Osterbrock 1989)

$$Q_{\star} = 4\pi \int_0^{r_s} n_{\text{p}} n_{\text{e}} \alpha_{\text{B}} r^2 dr \Rightarrow Q_{\star} = \frac{4}{3} \pi r_s^3 n_{\text{H I}}^2 \alpha_{\text{B}}, \quad (4)$$

for a neutral plasma, $n_{\text{p}} = n_{\text{e}} = n_{\text{H I}}$ of constant density, defining the Strömgren sphere.

For a star of effective temperature T_{\star} , we obtain the ionising photon rate from the integrated intensity of the Planck function,

³ Although it has been argued that the arms concentrate the gas without triggering star formation (Foyle et al. 2010). Furthermore, while Seigar & James (2002) find a correlation between spiral arm strength and star formation, Foyle et al. (2010) and Eden et al. (2013) find the inter-arm star formation rates to be similar to those in the arms. Compounding the issue further is the fact that the star formation rate is correlated with the molecular gas abundance, as traced through CO (Bigiel et al. 2008; Leroy et al. 2013), although the spiral arms do not appear to host elevated CO levels (Elmegreen & Elmegreen 1987; Dickey et al. 2009; Koda et al. 2016).

Table 1. Values of $\langle T_{\text{spin}}/f \rangle$ [K] at various impact parameters for the various column density profiles (Sects. 2.2.2 - 2.2.4).

Model	Fig.	Approximate radius/impact parameter [kpc]				
		5	12	15	20	30
Measured	3	1400^{+1400}_{-700}	—	2300^{+900}_{-700}	1100^{+500}_{-300}	at 25 kpc
Galactic – poly	7	5300^{+3100}_{-2000}	$15\,000^{+8000}_{-5000}$	7700^{+2300}_{-1800}	2700^{+500}_{-400}	250^{+50}_{-40}
– exponential	—	—	$16\,000^{+10000}_{-6000}$	2600^{+600}_{-500}	≥ 3300	320^{+80}_{-60}
Sample – poly	11	1800^{+1300}_{800}	6900^{+4000}_{-2500}	4100^{+1600}_{-1100}	3600^{+1100}_{-800}	460^{+110}_{-90}
– exponential	—	1900^{+1300}_{800}	6300^{+3700}_{-2300}	3300^{+1300}_{-900}	3000^{+900}_{-700}	1100^{+270}_{-220}
Simulated	14	1500^{+1000}_{600}	3300^{+1900}_{-1200}	1400^{+500}_{-400}	1200^{+400}_{-300}	180^{+40}_{-30}

Table 2. The estimated properties of stars of various effective temperatures, T_* . L_{MS} is the bolometric luminosity estimate from the temperature of a main sequence star, followed by the radius required to equate this to the bolometric intensity and finally the number of ionising photons per second.

T_* [K]	L_{MS} [L_{\odot}]	Radius [R_{\odot}]	Q_* [s^{-1}]
10000	46	2.3	7.8×10^{41}
20000	4200	5.4	2.7×10^{46}
30000	59 000	9.0	1.8×10^{48}
40000	4×10^5	13	2.0×10^{49}
50000	2×10^6	17	1.1×10^{50}

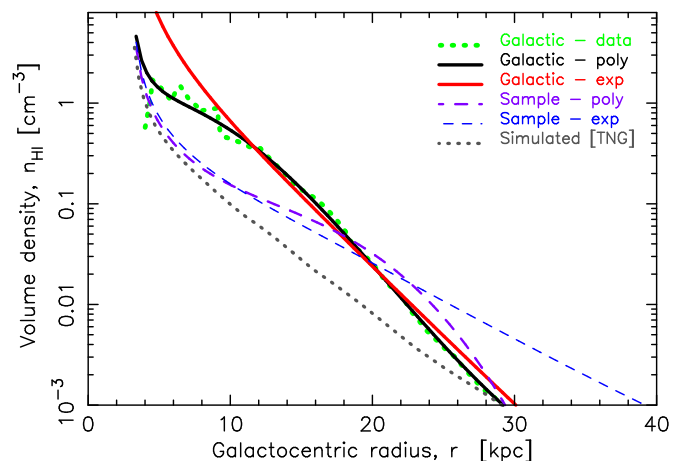
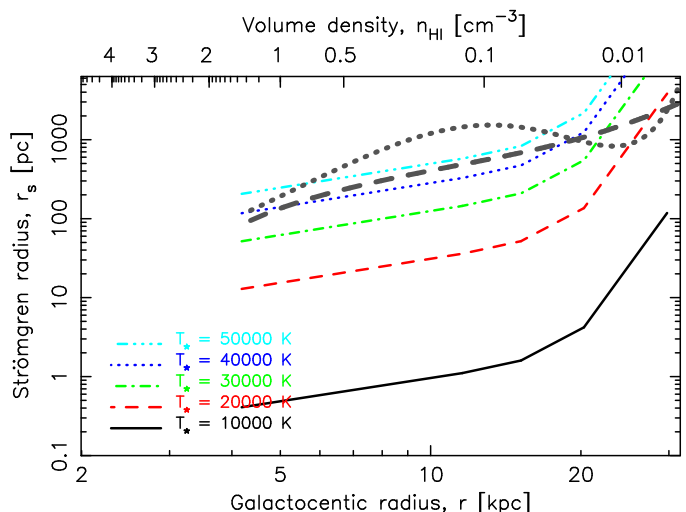
 I_{ν} ,

$$Q_* = 4\pi R_*^2 \int_{\nu_0}^{\infty} \frac{I_{\nu}}{h\nu} d\nu, \text{ where } I_{\nu} = \frac{2\pi h\nu^3}{c^2} \frac{1}{e^{h\nu/kT_*} - 1} \quad (5)$$

and $4\pi R_*^2$ is the surface area of the star. We estimate this by comparing the bolometric intensity, $I = \int_0^{\infty} I_{\nu} d\nu$, with the bolometric luminosity obtained from the main sequence ($\log_{10} L_{\text{MS}} = 6.50 \log_{10} T_* - 24.37$), giving the values of Q_* listed in Table 2.

Applying these to Equ. 4 yields the Strömgen radius of each star. For the radiative recombination rate coefficient, α_B , we assume that the electron temperature is equivalent to the spin temperature ($T_e = T_{\text{spin}}$). Arising from different heating/cooling processes, this is may not be justified although, given that $\alpha \propto \sqrt{T_e}$, the temperature dependence is not strong.⁴ From Equ. 4 we see that the Strömgen radius is dominated by the volume density, which we obtain at a given Galactocentric radius by assuming the log-polynomial $L - r$ profile of the sample (Fig. 15). These give the Strömgen radii shown in Fig. 16. Due to the decrease in gas density, for a homogeneous, dust-free medium, we see that the size of the sphere increases significantly with galactocentric radius.

In disc galaxies the star formation rate is found to increase with galactocentric radius (Muñoz-Mateos et al. 2007; Azzollini et al. 2009). This could be the result of the denser environments closer to the galactic centre suppressing the star formation (Boissier et al. 2007; Welikala et al. 2008). The outward growth of galactic discs would mean that the large radii are dominated by the younger (and more short-lived) stellar populations (Trujillo & Pohlen 2005; Muñoz-Mateos et al. 2007), giving a larger fraction of the more luminous stars (Table. 1). For the O-type stars ($T_* \geq 30\,000$ K), we see that the Strömgen radius

⁴ <http://amdpp.phys.strath.ac.uk/tamoc/DATA/RR/>

Fig. 15. Estimated volume densities for the various column density profiles obtained from the Galactic log-polynomial path length fit (Fig. 8).

Fig. 16. Strömgen radius versus the Galactocentric radius for stars of different effective temperatures obtained from the log-polynomial volume density fit to the sample (Fig. 15). The thick grey dotted curve shows the half-path length, $L/2$ (where $L = N_{\text{HI}}/n_{\text{HI}}$), for the mean of the sample and the dashed line for the Milky Way (Fig. 8).

for an individual star is comparable to the width of the H I disc at $r \geq 20$ kpc. Given the approximations, the values are uncertain, although it is apparent that, due to the decreasing density of the surrounding medium, the Strömgen radii exhibit a steep

increase, which is consistent with the gas being highly ionised at large impact parameters.

4. Conclusions

From the absorption of the 21-cm continuum from 90 sight-lines towards distant radio sources through the discs of nearby spiral galaxies, Curran et al. (2016) reported an anti-correlation between the abundance of cool, star-forming, gas and the galactocentric radius. Since the abundance of this gas normalised by the total H I column density gives a measure of the spin temperature, such an anti-correlation would be expected if the mean spin temperature were constant across the disc, as it is in the Milky Way (out to $r \approx 20$ kpc, Dickey et al. 2009). The correlation has, however, been disputed by subsequent data (increasing the number of sight-lines to 143, Borthakur 2016; Dutta et al. 2017).⁵ Including the new data in our analysis, we find the $\int \tau dv - \rho$ anti-correlation to increase in significance to $S(\tau) = 3.63\sigma$ from 3.31σ (Curran et al. 2016), thus demonstrating that, like all of the neutral atomic gas, the cold component decreases in abundance with galactocentric radius.

Comparing the mean 21-cm absorption strengths with the measured column densities, we find a possible peak in the spin temperature of $\langle T_{\text{spin}}/f \rangle \approx 2300$ K at $\rho \approx 14$ kpc, compared to $\langle T_{\text{spin}}/f \rangle \lesssim 1400$ K in the remainder of the stellar disc. We show, however, that the measured column densities obtained from the 21-cm emission are likely to suffer significant dilution due to the beam subtending beyond the disc. Applying better constrained column density profiles, we find:

- For the Galactic distribution, a peak of $\langle T_{\text{spin}}/f \rangle \approx 15000$ K at $\rho \approx 12$ kpc, with $\langle T_{\text{spin}}/f \rangle \gtrsim 3000$ K in the remainder of the disc.
- For the mean profile of the sample galaxies, where sufficiently high resolution data are available, a peak of $\langle T_{\text{spin}}/f \rangle \approx 7000$ K at $\rho \approx 12$ kpc, with $\langle T_{\text{spin}}/f \rangle \gtrsim 2000$ K in the remainder of the disc.
- For the mean of a simulated ensemble of spiral galaxies, a peak of $\langle T_{\text{spin}} \rangle \approx 3300$ K at $r \approx 12$ kpc, with $\langle T_{\text{spin}}/f \rangle \gtrsim 1000$ K in the remainder of the disc.

All of these spin temperatures are considerably higher than observed in the Milky Way ($T_{\text{spin}} \approx 250 - 400$ K, Dickey et al. 2009), being closer to those observed in other low redshift galaxies detected through the absorption of background quasar light, namely damped Lyman- α absorption systems (DLAs), where $T_{\text{spin}} \gtrsim 1000$ K at $z \approx 0$. At the peak of the star formation history at $z \sim 2$, however, the mean spin temperatures of the DLAs approach those in the Milky Way (Curran 2019).

We speculate that the elevated gas temperature at these radii may be coincident with the regions of highly ionised gas observed in some nearby spirals. At $r \gtrsim 10$ kpc, where $n_{\text{H I}} \lesssim 0.1 \text{ cm}^{-3}$, the radius of the H II region around each O-type star exceeds $r_s \sim 100$ pc, which is a significant fraction of the path length through the gaseous disc. Hence the presence of hot stars, in conjunction with the low gas densities, does indeed suggest that the gas is highly ionised at large Galactocentric radii.

Acknowledgements

I would like to thank the anonymous referee for their helpful feedback and Dylan Nelson for the IllustrisTNG data. This research has made use of the NASA/IPAC Extragalactic Database

(NED) which is operated by the Jet Propulsion Laboratory, California Institute of Technology, under contract with the National Aeronautics and Space Administration and NASA's Astrophysics Data System Bibliographic Service. This research has also made use of NASA's Astrophysics Data System Bibliographic Service and asurv Rev 1.2 (Lavalley et al. 1992), which implements the methods presented in Isobe et al. (1986).

References

- Allison, J. R. et al. 2020, MNRAS, submitted
 Azzollini, R., Beckman, J. E., & Trujillo, I. 2009, A&A, 501, 119
 Bahcall, J. N. & Ekers, R. D. 1969, ApJ, 157, 1055
 Bigiel, F., Leroy, A., Walter, F., et al. 2008, AJ, 136, 2846
 Boisse, P., Dickey, J. M., Kazes, I., & Bergeron, J. 1988, A&A, 191, 193
 Boissier, S., Gil de Paz, A., Boselli, A., et al. 2007, ApJS, 173, 524
 Borthakur, S. 2016, ApJ, 829, 128
 Borthakur, S., Momjian, E., Heckman, T. M., et al. 2014, ApJ, 98
 Borthakur, S., Tripp, T. M., Yun, M. S., et al. 2011, ApJ, 727, 52
 Borthakur, S., Tripp, T. M., Yun, M. S., et al. 2010, ApJ, 713, 131
 Carilli, C. L. & van Gorkom, J. H. 1992, ApJ, 399, 373
 Corbelli, E. & Schneider, S. E. 1990, ApJ, 356, 14
 Curran, S. J. 2012, ApJ, 748, L18
 Curran, S. J. 2019, MNRAS, 484, 3911
 Curran, S. J., Koribalski, B. S., & Bains, I. 2008, MNRAS, 389, 63
 Curran, S. J., Reeves, S. N., Allison, J. R., & Sadler, E. M. 2016, MNRAS, 459, 4136
 Dickey, J. M., Strasser, S., Gaensler, B. M., et al. 2009, ApJ, 693, 1250
 Dutta, R., Gupta, N., Srianand, R., & O'Meara, J. M. 2016, MNRAS, 456, 4209
 Dutta, R., Srianand, R., Gupta, N., et al. 2017, MNRAS, 465, 588
 Eden, D. J., Moore, T. J. T., Morgan, L. K., Thompson, M. A., & Urquhart, J. S. 2013, MNRAS, 431, 1587
 Elmegreen, B. G. & Elmegreen, D. M. 1987, ApJ, 320, 182
 Field, G. B. 1959, ApJ, 129, 536
 Foyle, K., Rix, H.-W., Walter, F., & Leroy, A. K. 2010, ApJ, 725, 534
 Gupta, N., Srianand, R., Bowen, D. V., York, D. G., & Wadadekar, Y. 2010, MNRAS, 408, 849
 Gupta, N., Srianand, R., Noterdaeme, P., Petitjean, P., & Muzahid, S. 2013, A&A, 558, A84
 Haschick, A. D. & Burke, B. F. 1975, ApJ, 200, L137
 Hodge, P. W. 1969, ApJ, 155, 417
 Hodge, P. W. & Kennicutt, Jr., R. C. 1983, ApJ, 267, 563
 Hwang, C.-Y. & Chiou, S.-H. 2004, ApJ, 600, 52
 Isobe, T., Feigelson, E., & Nelson, P. 1986, ApJ, 306, 490
 James, P. A., Bretherton, C. F., & Knapen, J. H. 2009, A&A, 501, 207
 Kalberla, P. M. W. & Dedes, L. 2008, A&A, 487, 951
 Kalberla, P. M. W., Dedes, L., Kerp, J., & Haud, U. 2007, A&A, 469, 511
 Kalberla, P. M. W. & Kerp, J. 2009, Ann. Rev. Astr. Ap., 47, 27
 Kanekar, N., Athreya, R. M., & Chengalur, J. N. 2002, A&A, 382, 838
 Koda, J., Scoville, N., & Heyer, M. 2016, ApJ, 823, 76
 Lavalley, M. P., Isobe, T., & Feigelson, E. D. 1992, in BAAS, Vol. 24, 839–840
 Leroy, A. K., Walter, F., Sandstrom, K., et al. 2013, AJ, 146, 19
 Lockman, F. J. 1976, ApJ, 209, 429
 McClure-Griffiths, N. M., Dickey, J. M., Gaensler, B. M., et al. 2005, ApJS, 158, 178
 Morgan, W. W., Whitford, A. E., & Code, A. D. 1953, ApJ, 118, 318
 Muñoz-Mateos, J. C., Gil de Paz, A., Boissier, S., et al. 2007, ApJ, 658, 1006
 Nelson, D., Springel, V., Pillepich, A., et al. 2019, Computational Astrophysics and Cosmology, 6, 2
 Osterbrock, D. E. 1989, Astrophysics of Gaseous Nebulae and Active Galactic Nuclei (Mill Valley, California: University Science Books)
 Peacock, J. A. 1999, Cosmological Physics (Cambridge: Cambridge University Press)
 Purcell, E. M. & Field, G. B. 1956, ApJ, 124, 542
 Reeves, S. N., Sadler, E. M., Allison, J. R., et al. 2015, MNRAS, 450, 926
 Reeves, S. N., Sadler, E. M., Allison, J. R., et al. 2016, MNRAS, 457, 2613
 Rohlfs, K. & Wilson, T. L. 2000, Tools of Radio Astronomy (Berlin: Springer-Verlag)
 Seigar, M. S. & James, P. A. 2002, MNRAS, 337, 1113
 Sofue, Y. 2018, PASJ, 70, 50
 Srianand, R., Gupta, N., Rahmani, H., et al. 2013, MNRAS, 428, 2198
 Stil, J. M., Taylor, A. R., Dickey, J. M., et al. 2006, AJ, 132, 1158
 Taylor, A. R., Gibson, S. J., Peracaula, M., et al. 2003, AJ, 125, 3145
 Toomre, A. 1963, ApJ, 138, 385
 Trujillo, I. & Pohlen, M. 2005, ApJ, 630, L17
 Walter, F., Brinks, E., de Blok, W. J. G., et al. 2008, AJ, 136, 2563
 Welikala, N., Connolly, A. J., Hopkins, A. M., Scranton, R., & Conti, A. 2008, ApJ, 677, 970
 Zwaan, M. A., Liske, J., Péroux, C., et al. 2015, MNRAS, 453, 1268

⁵ With one additional sight-line from Allison (2020).